Published in: Ind. Eng. Chem. Res. 2017, 56, 10134−10141

Contribution to Industrial & Engineering Chemistry Research

Syngas production by biogas reforming in a redox-stable and CO_2-tolerant oxygen transporting membrane reactor

Guanghu He,[a] Tianmiao Hu,[a,b] Hangyue Zhou,[a,b] Fangyi Liang,[a] Stefan Baumann,[c] Wilhelm A. Meulenberg,[c] and Heqing Jiang[a*]

[a] Qingdao Key Laboratory of Functional Membrane Material and Membrane Technology, Qingdao Institute of Bioenergy and Bioprocess Technology, Chinese Academy of Sciences, 266101 Qingdao, China

[b] University of Chinese Academy of Sciences, 100049 Beijing, China

[c] Institute of Energy and Climate Research (IEK-1), Forschungszentrum Jülich GmbH, D-52425 Jülich, Germany

* Corresponding author: jianghq@qibebt.ac.cn

Abstract

A novel membrane reactor consisting of $Ce_{0.9}Gd_{0.1}O_{2-\delta}$ − $Gd_{0.1}Sr_{0.9}Fe_{0.9}Ti_{0.1}O_{3-\delta}$ (CGO−GSFT) is used to combine air separation with biogas reforming in a single unit. The composite material CGO−GSFT was synthesized via a combined EDTA−citrate complexing sol-gel method. Characterization with XRD, SEM and EDXS revealed that the composite material was a two-phase fluorite-perovskite system with good compatibility and a homogeneous percolative network. XRD demonstrated that the CGO-GSFT membrane shows a good phase stability not only in CO_2 but also in simulated biogas atmosphere. Under the gradient of air/simulated biogas, the oxygen permeability and methane conversion was increased by either raising the operating temperature or increasing the CO_2 concentration. At 890 ˚C and a CH_4/CO_2 molar ratio of 1.5, an oxygen permeation flux of 1.1 cm^3 min^{-1} cm^{-2} through the CGO−GSFT membrane was achieved while methane conversion reached 83%, and remained stable for nearly 150 h before the measurement was intentionally stopped.

Keywords: biogas reforming, syngas, dual-phase oxygen transporting membrane, oxygen permeation, stability

Introduction

Rapid depletion of fossil fuels and increasingly stringent environmental regulations for greenhouse gases[1-2] are leading to an increased interest in the search of renewable resources as alternatives for syngas (a mixture of H_2 and CO) production and its further catalytic transformation into a great variety of products such as Fischer-Tropsch fuels, methanol and ammonia. Biogas, a mixture primarily composed of methane (60−70%), carbon dioxide (30−40%) and a small amount of H_2S, H_2O and siloxanes typically produced by anaerobic digestion of biogenic materials, is considered a promising alternative to fossil fuels and has attracted considerable attention from both energy and environmental viewpoints.[3] In addition to the direct use of biogas as a fuel for cooking and internal combustion engines,[4] biogas can be converted catalytically through the dry reforming of methane (R1) into syngas for producing high value chemicals. Thus, biogas reforming is considered to be a meaningful complementary route for syngas production without the involvement of fossil resources.

DRM: $CH_4 + CO_2 \rightarrow 2CO + 2H_2 \quad \Delta H_{298} = +206.2\ \text{kJ/mol}$ R1

POM: $CH_4 + 0.5O_2 \rightarrow CO + 2H_2 \quad \Delta H_{298} = -35.6\ \text{kJ/mol}$ R2

Dry reforming of methane (DRM) is a strongly endothermic reaction and needs a theoretical ratio of CH_4 to CO_2 of 1:1, as indicated in equation R1. However, the CO_2 concentration in biogas is less than 50% (usually 30−40%). To fully convert methane into syngas, additional air can be fed in together with the biogas, resulting in a

combination of DRM with partial oxidation of methane (POM, R2).[5-6] In this case, a portion of methane from the biogas will be converted to syngas via POM, in situ thus providing heat for the concurrent endothermic reaction between CO_2 and the rest of the methane from the biogas.[7] However, this co-feed process of biogas and air to syngas may be still subject to an additional oxygen-nitrogen separation plant because the downstream Fischer-Tropsch process usually needs nitrogen-free syngas. A significant part of the investment cost in the pure oxygen plant has so far limited biogas to fuel conversion technologies.

In our previous works, coupling oxygen transporting membranes (OTMs) with methane conversion to syngas or other chemicals used air directly as an oxidant, which enable the oxygen separation and catalytic oxidation in one unit.[8-9] Such a coupling strategy could simplify the operating process and reduce the cost. Consequently, it is reasonable to expect that the air separation plant in the conventional biogas reforming process could be eliminated by an OTM reactor. For practical applications, OTM materials must exhibit high oxygen permeability while maintaining structural and chemical stability under harsh working conditions (such as CO_2, CH_4, syngas *etc.*). Accordingly, the conversion of biogas to syngas means that most of OTMs doped by large amounts of Ba^{2+} in the A-site or $Co^{4+/3+}$ in the B-site of the perovskite structure such as $Ba_{0.5}Sr_{0.5}Co_{0.8}Fe_{0.2}O_{3-\delta}$,[10-11] $BaCo_{1-x-y}Fe_xNb_yO_{3-\delta}$ [12-13] and $BaCo_{1-x-y}Fe_xZr_yO_{3-\delta}$,[14] cannot be taken in consideration owing to their poor phase stability and chemical stability under a large oxygen partial pressure gradient, with one

side of the membrane exposed to air and the other side to CO_2 containing atmospheres or reducing atmosphere.[15-17]

Mixed conducting dual-phase OTMs[18-24] have attracted considerable attention in the past few decades since the two phases can be tailored separately as requested for a particular application. In particular, dual-phase membranes consisting of oxygen ionic conducting oxides and mixed ionic-electronic conducting oxides exhibit higher oxygen permeability than those of traditional dual-phase membranes (i.e. a mixture of ionic conducting oxides and pure electronic conducting oxides), together with high chemical stability in the presence of CO_2 in a wide temperature range[25] or under the condition of the POM reaction.[26] Based on this design concept of dual-phase membranes and the fact of the less flexible redox behavior of iron than cobalt,[27-28] in this work a new oxygen transporting membrane for simulated biogas reforming to produce syngas has been developed. The membrane comprises an oxygen ionic conducting oxide $Ce_{0.9}Gd_{0.1}O_{2-\delta}$ (CGO) with a fluorite structure and a mixed conducting oxide $Gd_{0.1}Sr_{0.9}Fe_{0.9}Ti_{0.1}O_{3-\delta}$ (GSFT) with a perovskite structure. This CGO−GSFT dual phase membrane demonstrates good oxygen permeability and considerable stability under simulated biogas reforming to syngas condition for about 150 h.

Experimental

Synthesis of the composite powders and membranes

The dual-phase oxides with composition of 60 mol% $Ce_{0.9}Gd_{0.1}O_{2-\delta}$ −40 mol% $Gd_{0.1}Sr_{0.9}Fe_{0.9}Ti_{0.1}O_{3-\delta}$ (60CGO−40GSFT) were synthesized via a one-pot method[29] with Ce, Gd, Sr and Fe metal nitrates and titanium butoxide (first dissolved in ethanol

and lactic acid). All the powders were calcined at 950 °C for 10 h in air and then pressed into disks under a pressure of 230 MPa. The disks were sintered at 1450 °C for 10 h in air to obtain gas-tight membranes with 15.4 mm in diameter and 0.7 mm in thickness.

Characterization of membrane materials

The crystal structures of the fresh and spent membranes were characterized by X-ray diffraction (XRD, D8-advance, Bruker, Germany) using Cu Kα radiation. The experimental diffraction patterns were collected by scanning in a 2θ range of 20−80° with an interval of 0.02°. The morphology and EDXS analysis of the membranes were determined by a Hitachi S-4800 field emission scanning electron microscope.

Biogas reforming performance of the dual-phase membranes reactor

Biogas reforming using a dual-phase CGO−GSFT oxygen permeable membrane was performed in a home-made membrane reactor.[30] A disk-shaped membrane was sealed onto an alumina tube using a glass ring (Schott 8252) at 1030 °C for 1 h. 0.3 g of commercial Ni_2O_3/Al_2O_3 catalyst (Süd Chemie AG) with a grain size of 0.3 – 0.5 mm diluted with SiO_2 powder was loaded on the biogas side of the membrane. After leakage testing under air/He gradient, oxygen permeation performances were examined based on two membrane disks, respectively. The oxygen permeation fluxes were well duplicated in two experiments. Simulated biogas diluted with helium (total 20 cm^3 min^{-1}) was fed to one side with packed catalyst (biogas side) and synthetic air with a flow rate of 100 cm^3 min^{-1} was fed to the other side (air side). The helium and carbon dioxide flow rates were controlled by gas mass flow controllers (Bronkhorst,

Germany). The methane and synthetic air flow rates were controlled by mass flow controllers (Seven Star, China). All flow rates were calibrated regularly by using a bubble flow meter. The gas composition of the outlet stream on the biogas side was analyzed using an on-line gas chromatography (GC, Aglient 7820B) equipped with HayeSep Q and Molsieve 5A modules. Appropriate sealing was confirmed by detecting the nitrogen tracer content of the outlet stream on the biogas side, which was only considered when the gas leakage was lower than 1 % of the permeate. Furthermore, performance stability study of the CGO−GSFT membrane exposed to simulated biogas/air gradient was carried out at 890 °C.

The oxygen permeation fluxes through the CGO−GSFT membranes were calculated from the amount of oxygen-containing species in the inlet and outlet streams on the biogas side. The oxygen permeation flux $J(O_2)$, methane conversion $X(CH_4)$ and CO selectivity S(CO) for biogas reforming were calculated using the following equations:

$$J(O_2) = \frac{F(CO,out) + 2F(CO_2,out) + F(H_2O,out) - 2F(CO_2,in)}{2A} \quad \text{(eq.1)}$$

$$X(CH_4) = (1 - \frac{F(CH_4,out)}{F(CH_4,in)}) \times 100\% \quad \text{(eq.2)}$$

$$S(CO) = (\frac{F(CO)}{F(CH_4,in) + F(CO_2,in) - F(CH_4,out) - F(CO_2,out)}) \times 100\% \quad \text{(eq.3)}$$

Where F_i is the flow rate of species i, and A is the effective area of the membrane.

Results and discussion

Structure and morphologies

Figure 1 shows the XRD patterns of the CGO−GSFT powder after calcining the precursor ash at 950 °C in air for 10 h and of dense membrane after sintering at 1450 °C in air for 10 h. For comparison, reference cubic fluorite (CGO) and perovskite ($SrFeO_{3-\delta}$) structure diffraction patterns are also indicated (ICDD 00-075-0161 and 00-034-0638, respectively). The composite material comprised only a CGO phase (space group 225: *Fm-3m*) and a GSFT phase (space group 221: *Pm-3m*), indicating that the two phases have good structural compatibility with each other. The good phase compatibility is also based on that the two phases have the same rare-earth element gadolinium.

Figure 2 shows the scanning electron microscopy (SEM) and energy-dispersive X-ray spectroscopy (EDXS) images of the sintered dual phase CGO−GSFT membrane. In Figure 2a, a homogeneous distribution of grains is observed. Further magnification (Figure 2b and Figure 2c) indicates that the dual-phase membrane is dense and no defects (cracks, pores) are visible. It is known that a high sintering temperature of about 1600 °C is necessary to obtain a dense CGO membrane.[31] Since the addition of iron-based perovskite oxides acting as a sintering agent can lower the sintering temperature of CGO,[32-33] dense CGO−GSFT membranes were obtained after sintering at only 1450 °C. The phase distribution of the membrane is shown by EDXS (Figure 2d-f). Figure 2d shows the color version EDXS where the green color is due to overlapping of the Gd, Sr, Fe and Ti signals, whereas the blue color derive from an average of the Ce and Gd signals. The Sr distributions in the GSFT grains (Figure 2e)

and Ce in the CGO grains (Figure 2f) indicate that the grains of the two phases are well separated with clear grain boundaries.

Thus, from the XRD patterns and SEM−EDXS images, the dual phase membrane with a GSFT perovskite phase and a CGO fluorite phase was successfully synthesized via a one-pot single-step procedure. The two phases were chemically compatible with each other and no reactions or impurities were discovered between them. A good network for oxygen ionic and electronic diffusion was formed in the CGO-GSFT composite membrane.

Phase stability of CGO−GSFT dual phase material

Considering the use of the CGO−GSFT membrane for biogas reforming to syngas at high temperatures, the membrane material must well tolerate CH_4 reduction and CO_2 corrosion. To evaluate its biogas tolerance, sintered CGO−GSFT membranes were exposed to various atmospheres at 850 °C for 24 h, including pure He, pure CO_2 and simulated biogas (30% CH_4 + 20% CO_2) balanced with He, as shown in Figure 3. Basically, the well-known problem of Fe-based OTM materials is poor stability because of the phase transformation from cubic structure to orthorhombic distorted perovskite or hexagonal structure at low temperatures.[34-35] On the other hand, CO_2 is known to be a corrosive gas to most of OTMs that usually contain high basicity elements such as Ba.[36] However, all the treated membrane samples in this work retained their dual phases CGO (cubic fluorite) and GSFT (cubic perovskite). In particular, no carbonate phase was observed in the sample after exposure to pure CO_2 at 850 °C for 24 h (Figure 3), indicating that CGO – GSFT membrane had a good CO_2

tolerance. This can be further supported by SEM-EDXS results. As shown in Figure S1 (see Supporting Information), the CGO-GSFT grains were visible and no obvious enrichment of carbonate at the grain boundaries was observed. This contrasts with the $Ce_{0.8}Gd_{0.2}O_{1.9}$ – $Gd_{0.2}Sr_{0.8}FeO_{3-\delta}$ membrane, and $SrCO_3$ phase was detected in this dual phase membrane under methane oxidation condition.[29] Thus, the improved CO_2 tolerance of CGO-GSFT membrane material should result from Ti doping which can reduce surface basicity of membrane surface and influence CO_2 adsorption at the membrane surface.[37] After exposure to simulated biogas atmosphere, both the cubic structure and phase composition remained unchanged, and no secondary phases resulting from the reduction of the transition metal ions in perovskite oxides[38] were detected by XRD, revealing the better reduction tolerance of CGO−GSFT dual-phase materials than that of cobalt based materials.[39-40] Considering that raw biogas also always contains a significant amount of impurities such as H_2S and H_2O, the phase stability of CGO – GSFT membranes exposed to 500 ppm H_2S and 3 vol.% H_2O atmospheres at 850 ˚C was investigated respectively (see Figure S2 in Supporting Information). According to the XRD patterns, the CGO-GSFT membrane exhibited a good chemical stability under a H_2O containing atmosphere. However, additional diffraction peaks assigned to the strontium sulfate phase[41] were observed from the H_2S-treated sample, indicating low sulfur tolerance of the CGO – GSFT membrane. Therefore, in practice biogas desulfurization is needed prior to converting biogas to syngas in membrane reactors, which is also a common method in other biogas utilization processes.[3] The above results suggest that the dual-phase CGO−GSFT

membrane is chemically stable in CO_2, simulated biogas and H_2O containing atmospheres, which is acceptable for the syngas production via the coupling of biogas reforming and air separation processes.

Conversion of biogas to syngas in a membrane reactor

The dual phase CGO−GSFT membrane with good CO_2 and reduction tolerance was successfully used as a reactor for the coupling of air separation and biogas reforming to syngas. As shown in Figure 4, the two sides of the CGO−GSFT membrane are applied by synthetic air and simulated biogas with varying carbon dioxide concentrations, respectively. Under this environment, oxygen molecules on the air side adsorb on the membrane surface and dissociate into oxygen ion species. These oxygen ions then diffuse through the bulk of the membrane via oxygen vacancies to the biogas side where they are consumed. Because oxygen ions are transported via lattice oxygen vacancies in the membrane, nitrogen is completely isolated on the air side and the syngas produced on the other side is nitrogen free. The enlarged image in Figure 4 schematically shows the expected series of catalytic reforming processes of simulated biogas for syngas production on the permeate side. Before reaching the membrane surface, dry reforming of methane with carbon dioxide (R1) first takes place in the top zone of the catalyst, i.e. Ni/Al_2O_3. The generated syngas will further move to the membrane surface and be oxidized by the permeated oxygen on the membrane surface (R3). At the same time, part of the permeated oxygen may also be consumed by methane combustion according to R4. The formed

H_2O and CO_2 will leave from the membrane surface and react with the excess methane to produce syngas (R1 and R5) before leaving the catalyst bed.

$$CO + H_2 + 2O^* \rightarrow H_2O + CO_2 \quad \text{R3}$$

$$CH_4 + 4O^* \rightarrow 2H_2O + CO_2 \quad \text{R4}$$

$$CH_4 + H_2O \rightarrow CO + 3H_2 \quad \text{R5}$$

Figure 5 presents the oxygen permeation flux (Figure 5a) and biogas reforming performance (Figure 5b) in the membrane reactor at 850 °C as a function of CO_2 concentration in simulated biogas with synthetic air as the feed gas. Also, the exit gas composition, CO_2 conversion and the mole balance of carbon and hydrogen are given in Table S1. Carbon and hydrogen balances were within 5% in all experiments, suggesting that carbon deposition was not obvious and no water presented in the products. In all cases, excepting without CO_2 introduction, the products from biogas reforming contain CH_4, CO, H_2, CO_2 and carrier gas (He). High conversion indicates that most of CO_2 in the simulated biogas was consumed. If only sending methane and helium, without any CO_2 were sent to the permeate side, the oxygen permeation flux through the membrane was 0.18 cm^3 min^{-1} cm^{-2} (Figure 5a), meanwhile CH_4 conversion was 10.6%, and syngas with a H_2/CO ratio of around 2 was obtained on the permeate side (Figure 5b), implying that methane was mainly converted to syngas on the other side. Compared to $Ce_{0.85}Sm_{0.15}O_{1.925}$ - $Sm_{0.6}Sr_{0.4}FeO_{3-\delta}$ dual-phase membrane,[42] the relatively lower oxygen flux of the CGO-GSFT membrane under air/methane gradient should be related mainly to the lower oxygen vacancy concentration due to Ti substitution for Fe in the GSFT oxide.[43-44] However, at the expense of oxygen permeability, Ti substitution in GSFT oxide could significantly improve the thermal and chemical stability of CGO – GSFT membranes under

reducing and CO_2 atmospheres. Upon feeding CO_2 into the methane stream, carbon dioxide and methane were first converted into hydrogen and carbon monoxide which can faster consume the permeated oxygen on the membrane surface compared to methane. As a result, the oxygen permeability of the membrane was significantly improved due to the larger driving force. For example, when the CO_2 concentration in the stream was 5 vol% (CH_4/CO_2 feed ratio of 6), a higher oxygen permeation flux of about 0.33 cm^3 min^{-1} cm^{-2} was obtained, which is nearly twice as high as the flux of diluted methane alone as the sweep gas and more than three times higher than the flux of helium as the sweep gas (see Supporting Information Figure S3). At the same time, CH4 conversion increased to above 25% which was higher than the equilibrium conversion for the DRM reaction, indicating that other methane conversion reactions such as POM took place on the methane side. Furthermore, no steam was detected in the exit gases (Supporting information Table S1), suggesting that the H_2O formed on the membrane surface was converted fully by steam reforming (R5). In an earlier study, Evan et al. also found that steam reforming of methane to syngas can serve as an adjunct during biogas reforming,[45] Such a supplementary role of steam reforming could limit the presence of water in the final products. Accordingly, if CH_4/CO_2 feed ratio exceeds 1.0 by increasing the methane flow rate or concentration of CH_4, the intermediate water can be consumed by the excess methane, and the possibility of water presence in the product stream will be significantly reduced. However, it should be pointed out that too much increase of methane flow rate will significantly decrease the residence time in the catalyst bed, the formed water might leave the catalyst bed very quickly before being consumed by steam reforming of methane and present in the final product stream.

With further increasing CO_2 concentration in the gas stream, the oxygen permeation flux and the amount of syngas obtained are expected to increase. As shown in Figure 5a, the oxygen permeation flux increased gradually from 0.33 to 1.0 cm^3 min^{-1} cm^{-2} when the CO_2 concentration was increased from 5 vol.% to 20 vol.%. Accordingly, the CH_4 conversion in the simulated biogas stream was enhanced to approximately 82% (Figure 5b). At the same time, the H_2/CO ratio decreased gradually and then stabilized at around 1.2, indicating that the DRM and POM reactions took place simultaneously on the biogas side of the membrane reactor.

Figure 6 shows the temperature dependence of CH_4 conversion, CO selectivity and oxygen permeation flux with simulated biogas consisting of 30 vol.% CH_4 and 20 vol.% CO_2 (CH_4/CO_2 feed ratio of 1.5). Each temperature was held for about 1 h and the corresponding data points were recorded at least three times to ensure the accuracy of the results. It can be seen that CH_4 conversion increased from 79 to 83%, CO selectivity increased from 96 to 99% and oxygen permeation flux increased from 0.6 to 1.1 cm^3 min^{-1} cm^{-2} when the temperatures were increased from 830 to 890 °C. For simulated biogas with a specific CH_4/CO_2 ratio of 1.5, the increase in oxygen permeation flux with temperature spontaneously led to an increase in methane conversion. Furthermore, the increase of CO selectivity with raising temperatures and the fact that no water was detected in the products suggested that the permeated oxygen was less than the needed for the stoichiometric methane conversion reactions in the present study.

With good chemical stability and high oxygen permeability, the performance of the CGO−GSFT dual phase membrane reactor for biogas reforming was investigated as a function of time. Figure 7 presents the behavior of the CGO−GSFT dual phase membrane reactor as a function of time in which one side was exposed to simulated biogas (CH_4/CO_2 = 1.5) and synthetic air was fed to the other side. During a period of nearly 150 h, approximately 1.03 cm^3 min^{-1} cm^{-2} of oxygen permeation flux and more than 80% of methane conversion as well as nearly 100% of carbon monoxide selectivity were obtained at 890 ˚C. In this period, the CGO−GSFT membrane operated steadily and no fracture occurred. Furthermore, there was no ignition step in this membrane reactor, which is different from the induction process observed at the initial stage of POM.[46] It should be noted that the first data point was collected after a 2-hour activation stage of methane feeding into the reactor (Supporting Information, Figure S4). During that time Ni species in the catalyst were activated to metallic Ni^0.[47] Following the activation period, a steady-state conversion of simulated biogas to syngas was achieved via catalytic dry reforming and partial oxidation of methane in the membrane reactor. The activated oxygen species (e.g. O^{2-}, O^-, O_2^-, O_2^{2-})[48-50] at the membrane surface on the permeate side could increase CH_4 conversion and improve biogas utilization.

After the long-term operation, the phase composition and morphology of the membrane were characterized by XRD and SEM-EDXS. The diffraction peaks of CGO and GSFT phases for the spent membrane still existed, indicating that the CGO-GSFT membrane was stable under biogas reforming condition (Supporting

information Figure S5). In addition, the weak peaks observed around 27° (2θ) were assigned to graphite formed by coke deposition, as reported for the $Ce_{0.85}Sm_{0.15}O_{1.925}$ − $Sm_{0.6}Sr_{0.4}FeO_{3-\delta}$ dual phase membrane exposed to POM reaction condition.[42] Figure 8 shows SEM images of the surface on the biogas side and cross-section exposed to air of the spent membrane operated for over 140 h. Compared with the fresh membrane (Figure 2), the CGO and GSFT grains in the spent membrane were less easily visible, as shown in Figure 8a. This may be attributed to a combination of three causes including carbon deposition,[42] contamination caused by Ni-Al_2O_3 catalyst loading on the top of the membrane, and sintering during biogas reforming which enables the grains to be more closely packed.[51] The SEM-EDXS images (Figure 8b and Figure S6 in Supporting Information) for the cross-section of the spent membrane shows that the membrane remains dense after long-term operation, indicating the good stability of the CGO−GSFT membrane. With respect to the cobalt-containing membrane in our previous work,[40] we demonstrated the coupling of water splitting and ethane dehydrogenation in a $BaCo_xFe_yZr_{1-x-y}O_{3-\delta}$ membrane reactor and observed Co-enriched particles on the spent membrane surface. Cobalt extraction by reduction of cobalt from the perovskite structure led to membrane performance degradation. All this information indicates that the Co-free CGO−GSFT dual phase membrane has a high tolerance for reducing atmosphere and exhibits high potential for integration with biogas reforming for syngas production. However, in order to meet the practical operation conditions and commercialization purposes, future work regarding this membrane in biogas reforming should focus on membrane configuration, membrane

reactor performance in raw biogas as well as the process integration of membrane reactor with pre-treatment systems of biogas.

Conclusions

The present study experimentally demonstrated a way for producing syngas from biogas reforming in oxygen transporting membrane reactors. The membranes were made of a fluorite CGO phase as the oxygen ionic conductor and a perovskite GSFT phase as the mixed ionic-electronic conductor. The characterization results revealed that the CGO and GSFT phases formed a percolative network and had good structural compatibility with each other. CGO−GSFT dual phase membranes exhibited high chemical stability after a 24-hour exposure treatment by He, CO_2 or simulated biogas. The experimental results show that the syngas produced in CGO−GSFT membrane reactor was virtually free of nitrogen from the air side, and the CH_4 conversion increased with enhancing oxygen permeation flux by either feeding more CO_2 to the permeate side or increasing operating temperature. When CH_4/CO_2 ratio was 1.5, an oxygen permeation flux of 1.1 cm^3 min^{-1} cm^{-2} was obtained at 890 °C while CH_4 conversion reached a maximum at 83%. Under the same condition, this CGO−GSFT membrane reactor was operated steadily for nearly 150 h. SEM results indicated that the spent membrane retained its dual-phase structure and integrity. These results reveal that CGO−GSFT has a great application potential for reforming biogas to syngas.

Acknowledgements

The authors would like to acknowledge financial support from the National Natural Science Foundation of China (21506237, 21471156), the Shandong Provincial Natural Science Foundation, China (BS2015NJ002), China Postdoctoral Science Foundation (2015M570617), the State Key Laboratory of Coal Conversion (No: J15-16-907), and the project of the Science and Technology Development Program in Shandong Province (2014GSF117031).

Supporting Information

Exit gas composition, CO_2 conversion, mole balance of carbon and hydrogen of simulated biogas reforming into syngas via the CGO-GSFT membrane reactor. SEM-EDXS images and XRD pattern of CGO-GSFT membrane exposed to CO_2. XRD patterns of CGO−GSFT membranes after treatment under H_2S or H_2O containing atmospheres. Oxygen permeation fluxes of dual phase membrane under different conditions. Oxygen permeation flux during activation stage through CGO-GSFT membrane. XRD patterns of fresh and spent CGO-GSFT membranes. EDXS images of the spent membrane exposed to air.

References

(1) Jakob, M.; Hilaire, J. Climate science: Unburnable fossil-fuel reserves. *Nature* **2015**, *517*, 150.

(2) Ukaew, S.; Shi, R.; Lee, J. H.; Archer, D. W.; Pearlson, M.; Lewis, K. C.; Bregni, L.; Shonnard, D. R. Full chain life cycle assessment of greenhouse gases and energy demand for canola-derived jet fuel in north dakota, United States. *ACS Sustain. Chem. Eng.* **2016**, *4*, 2771.

(3) Yang, L.; Ge, X.; Wan, C.; Yu, F.; Li, Y. Progress and perspectives in converting biogas to transportation fuels. *Renew. Sustain. Energy Rev.* **2014**, *40*, 1133.

(4) Chen, L.; Shiga, S.; Araki, M. Combustion characteristics of an SI engine fueled with H_2-CO blended fuel and diluted by CO_2. *Int. J. Hydrogen Energy* **2012**, *37*, 14632.

(5) Kohn, M. P.; Castaldi, M. J.; Farrauto, R. J. Auto-thermal and dry reforming of landfill gas over a Rh/γAl_2O_3 monolith catalyst. *App. Catal. B* **2010**, *94*, 125.

(6) Zinoviev, S.; Müller-Langer, F.; Das, P.; Bertero, N.; Fornasiero, P.; Kaltschmitt, M.; Centi, G.; Miertus, S. Next-generation biofuels: Survey of emerging technologies and sustainability issues. *ChemSusChem* **2010**, *3*, 1106.

(7) Bhavani, A. G.; Kim, W. Y.; Kim, J.Y.; Lee, J. S. Improved activity and coke resistance by promoters of nanosized trimetallic catalysts for autothermal carbon dioxide reforming of methane. *App. Catal. A* **2013**, *450*, 63.

(8) Jiang, H.; Liang, F.; Czuprat, O.; Efimov, K.; Feldhoff, A.; Schirrmeister, S.; Schiestel, T.; Wang, H.; Caro, J. Hydrogen production by water dissociation in surface-modified

$BaCo_xFe_yZr_{1-x-y}O_{3-\delta}$ hollow-fiber membrane reactor with improved oxygen permeation. *Chem-Eur. J.* **2010**, *16*, 7898.

(9) Cao, Z.; Jiang, H.; Luo, H.; Baumann, S.; Meulenberg, W. A.; Assmann, J.; Mleczko, L.; Liu, Y.; Caro, J. Natural gas to fuels and chemicals: Improved methane aromatization in an oxygen-permeable membrane reactor. *Angew. Chem. Int. Ed.* **2013**, *52*, 13794.

(10) Shao, Z.; Dong, H.; Xiong, G.; Cong, Y.; Yang, W. Performance of a mixed-conducting ceramic membrane reactor with high oxygen permeability for methane conversion. *J. Membr. Sci.* **2001**, *183*, 181.

(11) Mueller, D. N.; De Souza, R. A.; Yoo, H. I.; Martin, M. Phase stability and oxygen nonstoichiometry of highly oxygen-deficient perovskite-type oxides: A case study of $(Ba,Sr)(Co,Fe)O_{3-\delta}$. *Chem. Mater.* **2012**, *24*, 269.

(12) Yi, J.; Weirich, T. E.; Schroeder, M. CO_2 corrosion and recovery of perovskite-type $BaCo_{1-x-y}Fe_xNb_yO_{3-\delta}$ membranes. *J. Membr. Sci.* **2013**, *437*, 49.

(13) Wu, C.; Wang, H.; Zhang, X.; Zhang, Y.; Ding, W.; Sun, C. Microstructure evolution and oxidation states of Co in perovskite-type oxide $Ba_{1.0}Co_{0.7}Fe_{0.2}Nb_{0.1}O_{3-\delta}$ annealed in CO_2 atmosphere. *J. Energy Chem.* **2014**, *23*, 575.

(14) Jiang, H.; Wang, H.; Werth, S.; Schiestel, T.; Caro, J. Simultaneous production of hydrogen and synthesis gas by combining water splitting with partial oxidation of methane in a hollow-fiber membrane reactor. *Angew. Chem. Int. Ed.* **2008**, *47*, 9341.

(15) Zhu, J.; Guo, S.; Chu, Z.; Jin, W. CO_2-tolerant oxygen-permeable perovskite-type membranes with high permeability. *J. Mater. Chem. A* **2015**, *3*, 22564.

(16) Thursfield, A.; Metcalfe, I. S. Methane oxidation in a mixed ionic-electronic conducting ceramic hollow fibre reactor module. *J. Solid State Electrochem.* **2006**, *10*, 604.

(17) Lobera, M. P.; Escolástico, S.; Garcia-Fayos, J.; Serra, J. M. Ethylene production by ODHE in catalytically modified $Ba_{0.5}Sr_{0.5}Co_{0.8}Fe_{0.2}O_{3-\gamma}$ membrane reactors. *ChemSusChem* **2012**, *5*, 1587.

(18) Liu, H.; Tan, X.; Pang, Z.; Diniz da Costa, J.C.; Lu, G. Q.; Liu, S. Novel dual structured mixed conducting ceramic hollow fibre membranes. *Sep. Purif. Tech.* **2008**, *63*, 243.

(19) Liu, T.; He, W.; Huang, H.; Wang, S.; Bouwmeester, H. J. M.; Chen, C. $Ce_{0.8}Sm_{0.2}O_{1.9}$–$La_{0.8}Sr_{0.2}Cr_{0.5}Fe_{0.5}O_{3-\delta}$ dual-phase hollow fiber membranes permeated under different gradients. *Ind. Eng. Chem. Res.* **2014**, *53*, 6131.

(20) Xue, J.; Liao, Q.; Wei, Y.; Li, Z.; Wang, H. A CO_2-tolerance oxygen permeable $60Ce_{0.9}Gd_{0.1}O_{2-\delta}$-$40Ba_{0.5}Sr_{0.5}Co_{0.8}Fe_{0.2}O_{3-\delta}$ dual phase membrane. *J. Membr. Sci.* **2013**, *443*, 124.

(21) Luo, H.; Efimov, K.; Jiang, H.; Feldhoff, A.; Wang, H.; Caro, J. CO_2-stable and cobalt-free dual-phase membrane for oxygen separation. *Angew. Chem. Int. Ed.* **2011**, *50*, 759.

(22) Guo, S.; Liu, Z.; Zhu, J.; Jiang, X.; Song, Z.; Jin, W. Highly oxygen-permeable and CO_2-stable $Ce_{0.8}Sm_{0.2}O_{2-\delta}$-$SrCo_{0.9}Nb_{0.1}O_{3-\delta}$ dual-phase membrane for oxygen separation. *Fuel Process.Technol.* **2016**, *154*, 19.

(23) Othman, N. H.; Wu, Z.; Li, K. $Bi_{1.5}Y_{0.3}Sm_{0.2}O_{3-\delta}$-based ceramic hollow fibre membranes for oxygen separation and chemical reactions. *J. Membr. Sci.* **2013**, *432*, 58.

(24) Garcia-Fayos, J.; Balaguer, M.; Serra, J. M. Dual-phase oxygen transport membranes for stable operation in environments containing carbon dioxide and sulfur dioxide. *ChemSusChem* **2015**, *8*, 4242.

(25) Wang, Z.; Sun, W.; Zhu, Z.; Liu, T.; Liu, W. A novel cobalt-free, CO_2-stable, and reduction-tolerant dual-phase oxygen-permeable membrane. *ACS Appl. Mater. Inter.* **2013**, *5*, 11038.

(26) Wang, B.; Yi, J.; Winnubst, L.; Chen, C. Stability and oxygen permeation behavior of $Ce_{0.8}Sm_{0.2}O_{2-\delta}$-$La_{0.8}Sr_{0.2}CrO_{3-\delta}$ composite membrane under large oxygen partial pressure gradients. *J. Membr. Sci.* **2006**, *286*, 22.

(27) Lu, Y.; Zhao, H.; Chang, X.; Du, X.; Li, K.; Ma, Y.; Yi, S.; Du, Z.; Zheng, K.; Świerczek, K. Novel cobalt-free $BaFe_{1-x}Gd_xO_{3-\delta}$ perovskite membranes for oxygen separation. *J. Mater. Chem. A* **2016**, *4*, 10454.

(28) Zhang, C.; Tian, H.; Yang, D.; Sunarso, J.; Liu, J.; Liu, S. Enhanced CO_2 resistance for robust oxygen separation through tantalum-doped perovskite membranes. *ChemSusChem* **2016**, *9*, 505.

(29) Zhu, X.; Yang, W. Composite membrane based on ionic conductor and mixed conductor for oxygen permeation. *AIChE J.* **2008**, *54*, 665.

(30) Luo, H.; Jiang, H.; Efimov, K.; Liang, F.; Wang, H.; Caro, J. CO_2-tolerant oxygen-permeable Fe_2O_3-$Ce_{0.9}Gd_{0.1}O_{2-\delta}$ dual phase membranes. *Ind. Eng. Chem. Res.* **2011**, *50*, 13508.

(31) Pérez-Coll, D.; Ruiz-Morales, J. C.; Marrero-López, D.; Núñez, P.; Frade, J. R. Effect of sintering additive and low temperature on the electrode polarization of CGO. *J. Alloy. Compd.* **2009**, *467*, 533.

(32) Mori, M.; Suda, E.; Pacaud, B.; Murai, K.; Moriga, T. Effect of components in electrodes on sintering characteristics of $Ce_{0.9}Gd_{0.1}O_{1.95}$ electrolyte in intermediate-temperature solid oxide fuel cells during fabrication. *J. Power Sources* **2006**, *157*, 688.

(33) Kaiser, A.; Foghmoes, S. P.; Pećanac, G.; Malzbender, J.; Chatzichristodoulou, C.; Glasscock, J. A.; Ramachandran, D.; Ni, D. W.; Esposito, V.; Søgaard, M.; Hendriksen, P. V. Design and optimization of porous ceramic supports for asymmetric ceria-based oxygen transport membranes. *J. Membr. Sci.* **2016**, *513*, 85.

(34) Kida, T.; Takauchi, D.; Watanabe, K.; Yuasa, M.; Shimanoe, K.; Teraoka, Y.; Yamazoe, N. Oxygen permeation properties of partially A-site substituted $BaFeO_{3-\delta}$ perovskites. *J. Electrochem. Soc.* **2009**, *156*, 156.

(35) Kida, T.; Yamasaki, A.; Watanabe, K.; Yamazoe, N.; Shimanoe, K. Oxygen-permeable membranes based on partially B-site substituted $BaFe_{1-y}M_yO_{3-\delta}$ (M=Cu or Ni). *J. Solid State Chem.* **2010**, *183*, 2426.

(36) Arnold, M.; Wang, H.; Feldhoff, A. Influence of CO_2 on the oxygen permeation performance and the microstructure of perovskite-type $(Ba_{0.5}Sr_{0.5})(Co_{0.8}Fe_{0.2})O_{3-\delta}$ membranes. *J. Membr. Sci.* **2007**, *293*, 44.

(37) Zeng, Q.; Zuo, Y. B.; Fan, C. G.; Chen, C. S. CO_2-tolerant oxygen separation membranes targeting CO_2 capture application. *J. Membr. Sci.* **2009**, *335*, 140.

(38) Xu, S. J.; Thomson, W. J. Stability of $La_{0.6}Sr_{0.4}Co_{0.2}Fe_{0.8}O_{3-\delta}$ perovskite membranes in reducing and nonreducing environments. *Ind. Eng. Chem. Res*. **1998**, *37*, 1290.

(39) Bouwmeester, H. J. M. Dense ceramic membranes for methane conversion. *Catal. Today* **2003**, *82*, 141.

(40) Jiang, H.; Cao, Z.; Schirrmeister, S.; Schiestel, T.; Caro, J. A coupling strategy to produce hydrogen and ethylene in a membrane reactor. *Angew. Chem. Int. Ed.* **2010**, *49*, 5656.

(41) Liu, Y.; Zhu, X.; Li, M.; Liu, H.; Cong, Y.; Yang, W. Stabilization of low-temperature degradation in mixed ionic and electronic conducting perovskite oxygen permeation membranes. *Angew. Chem. Int. Ed.* **2013**, *52*, 3232.

(42) Zhu, X.; Li, Q.; He, Y.; Cong, Y.; Yang, W. Oxygen permeation and partial oxidation of methane in dual-phase membrane reactors. *J. Membr. Sci.* **2010**, *360*, 454.

(43) Xu, N.; Zhao, H.; Shen, Y.; Chen, T.; Ding, W.; Lu, X.; Li, F. Structure, electrical conductivity and oxygen permeability of $Ba_{0.6}Sr_{0.4}Co_{1-x}Ti_xO_{3-\delta}$ ceramic membranes. *Sep. Purif. Technol.* **2012**, *89*, 16.

(44) Schulz, M.; Kriegel, R.; Kämpfer, A. Assessment of CO_2 stability and oxygen flux of oxygen permeable membranes. *J. Membr. Sci.* **2011**, *378*, 10.

(45) Evans, S. E.; Good, O. J.; Staniforth, J. Z.; Ormerod, R. M.; Darton, R. J. Overcoming carbon deactivation in biogas reforming using a hydrothermally synthesised nickel perovskite catalyst. *RSC Adv.* **2014**, *4*, 30816.

(46) Li, Q.; Zhu, X.; He, Y.; Yang, W. Partial oxidation of methane in $BaCe_{0.1}Co_{0.4}Fe_{0.5}O_{3-\delta}$ membrane reactor. *Catal. Today* **2010**, *149*, 185.

(47) Yuan, K.; Zhong, J. Q.; Zhou, X.; Xu, L.; Bergman, S. L.; Wu, K.; Xu, G. Q.; Bernasek, S. L.; Li, H. X.; Chen, W. Dynamic oxygen on surface: Catalytic intermediate and coking barrier in the modeled CO_2 reforming of CH_4 on Ni (111). *ACS Catal.* **2016**, *6*, 4330.

(48) Palmer, M. S.; Neurock, M.; Olken, M. M. Periodic density functional theory study of methane activation over La_2O_3: Activity of O^{2-}, O^-, O_2^{2-}, oxygen point defect, and Sr^{2+}-doped surface sites. *J. Am. Chem. Soc.* **2002**, *124*, 8452.

(49) Chen, H. T.; Raghunath, P.; Lin, M. C. Computational investigation of O_2 reduction and diffusion on 25% Sr-doped $LaMnO_3$ cathodes in solid oxide fuel cells. *Langmuir* **2011**, *27*, 6787.

(50) Setvín, M.; Aschauer, U.; Scheiber, P.; Li, Y. F.; Hou, W.; Schmid, M.; Selloni, A.; Diebold, U. Reaction of O_2 with subsurface oxygen vacancies on TiO_2 anatase (101), *Science* **2013**, *341*, 988.

(51) Yang, N. T.; Kathiraser, Y.; Kawi, S. $La_{0.6}Sr_{0.4}Co_{0.8}Ni_{0.2}O_{3-\delta}$ hollow fiber membrane reactor: Integrated oxygen separation – CO_2 reforming of methane reaction for hydrogen production. *Int. J. Hydrogen Energy* **2013**, *38*, 4483.

Figure Captions

Figure 1. XRD patterns of the dual-phase 60CGO−40GSFT powder calcined at 950 °C for 10 h and the dual-phase membrane sintered at 1450 °C for 10 h.

Figure 2. SEM (a, b, c) and EDXS (d, f) images of the 60CGO−40GSFT dual phase membrane after sintering at 1450 °C in air for 10 h. For the EDXS mapping in d, superimpositions of the Ce-Lα, Ce-Lβ, Gd-Lα, Gd-Lβ (blue) and Gd-Lα, Gd-Lβ, Sr-Lα, Fe-Kα, Fe-Kβ and Ti- Kα (green) signals were used.

Figure 3. X-ray diffraction patterns of CGO−GSFT dual phase membranes before and after exposure to various atmospheres at 850 °C for 24 h.

Figure 4. Concept of syngas production from catalytic biogas reforming in CGO−GSFT dual phase oxygen transporting membrane reactor.

Figure 5. Oxygen permeation fluxes (a), CH_4 conversion (X_{CH4}), CO selectivity (S_{CO}) and H_2/CO ratio (b) through 0.7 mm thick membrane by exposing one side to air (100 cm^3 min^{-1}) and the other side to He-CH_4-CO_2 (total 20 cm^3 min^{-1}) with a CH_4 concentration of 30% and a CO_2 concentration of 0%, 5%, 10%, 15% and 20%. Temperature: 850 ˚C.

Figure 6. Influence of temperature on the CH_4 conversion (X_{CH4}), CO selectivity (S_{CO}), and oxygen permeation flux (J_{O2}) through the 60CGO−40GSFT dual phase membrane in the coupling of biogas reforming and air separation. Conditions: 100 cm^3 min^{-1} air as feed gas, 20 cm^3 min^{-1} simulated biogas (He-CH_4-CO_2) as sweep gas with CH_4 concentration of 30% and CO_2 concentration of 20%. Membrane thickness: 0.7 mm.

Figure 7. Time-dependence of CH_4 conversion (X_{CH4}), CO selectivity (S_{CO}) and oxygen

permeation flux (J_{O2}) in the CGO−GSFT dual phase membrane reactor, Conditions: 100 cm^3 min^{-1} air as feed gas, 20 cm^3 min^{-1} simulated biogas (He-CH_4-CO_2) as sweep gas with CH_4 concentration of 30% and CO_2 concentration of 20%. Membrane thickness: 0.7 mm, Temperature: 890 ˚C.

Figure 8. The SEM micrographs of the membrane surface on the biogas side (a) and cross-section (b) of the spent membrane exposed to air after biogas reforming for nearly 150 h.

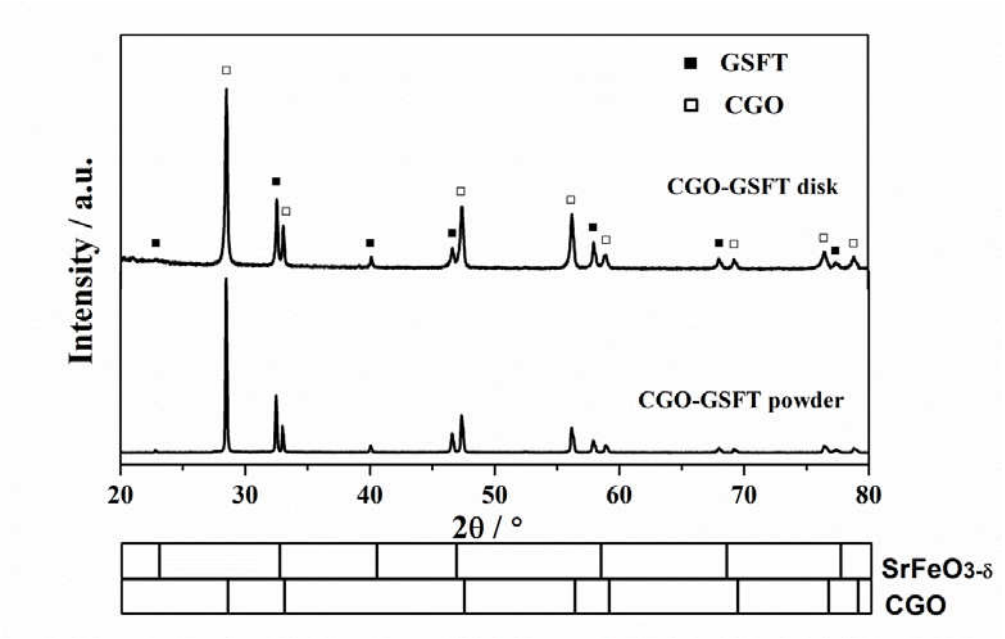

Figure 1. XRD patterns of the dual-phase 60CGO−40GSFT powder calcined at 950 °C for 10 h and the dual-phase membrane sintered at 1450 °C for 10 h.

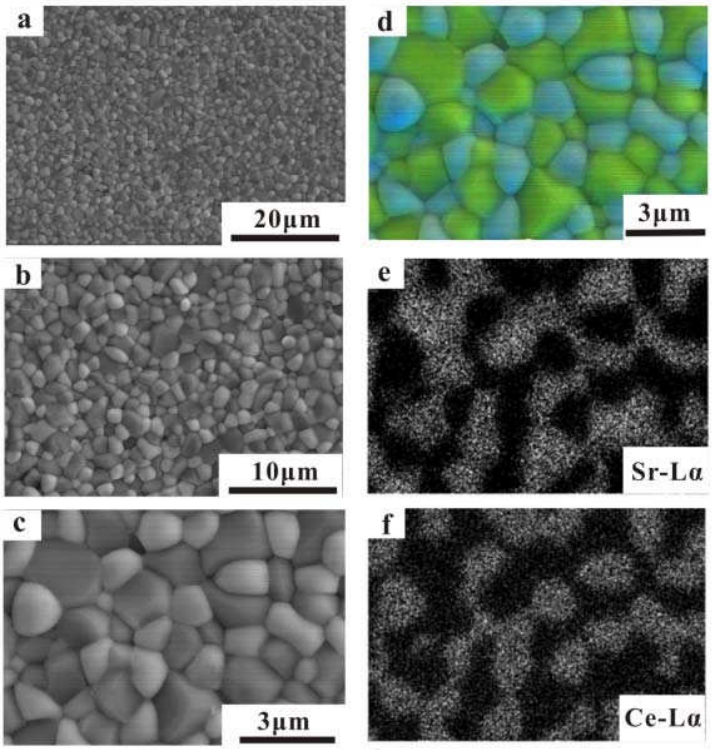

Figure 2. SEM (a, b, c) and EDXS (d, f) images of the 60CGO−40GSFT dual phase membrane after sintering at 1450 °C in air for 10 h. For the EDXS mapping in d, superimpositions of the Ce-Lα, Ce-Lβ, Gd-Lα, Gd-Lβ (blue) and Gd-Lα, Gd-Lβ, Sr-Lα, Fe-Kα, Fe-Kβ and Ti- Kα (green) signals were used.

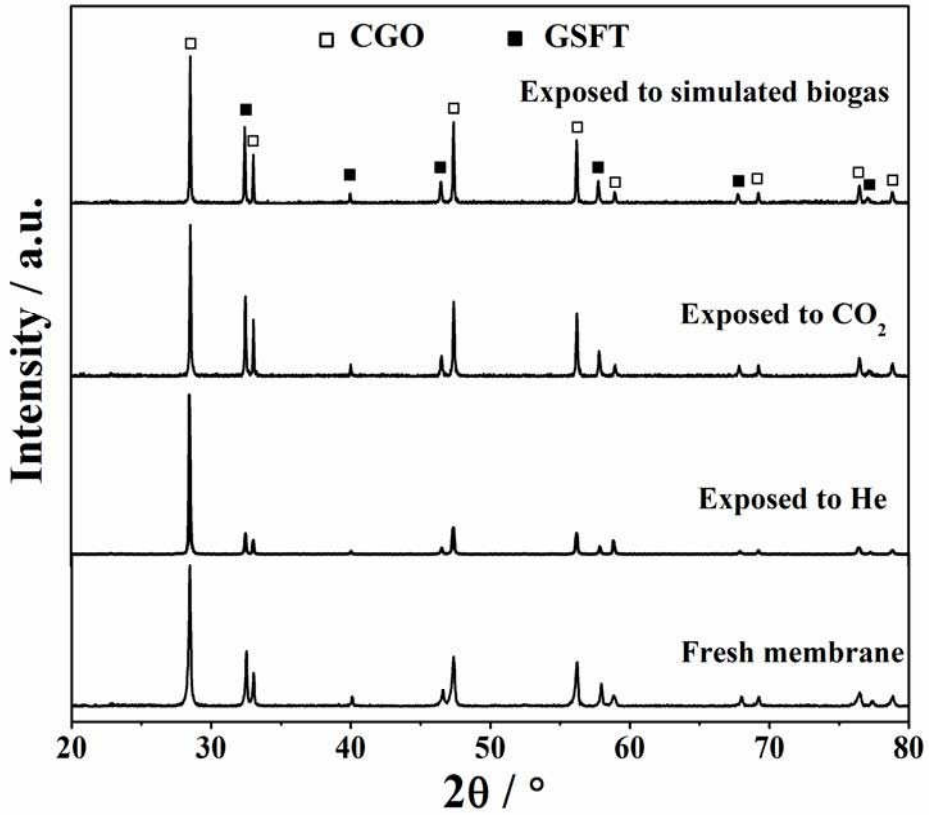

Figure 3. X-ray diffraction patterns of CGO−GSFT dual phase membranes before and after exposure to various atmospheres at 850 °C for 24 h.

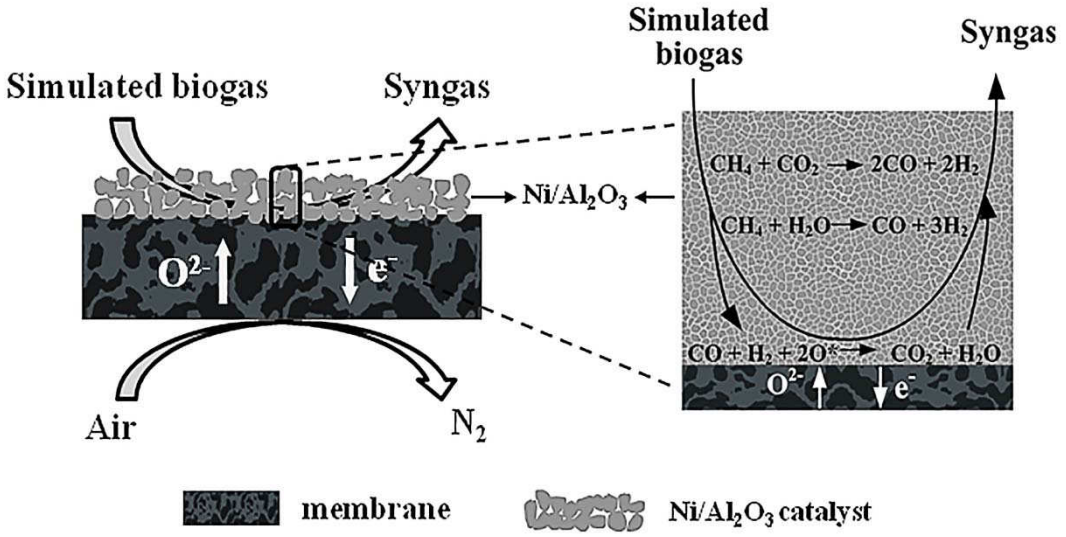

Figure 4. Concept of syngas production from catalytic biogas reforming in CGO−GSFT dual phase oxygen transporting membrane reactor.

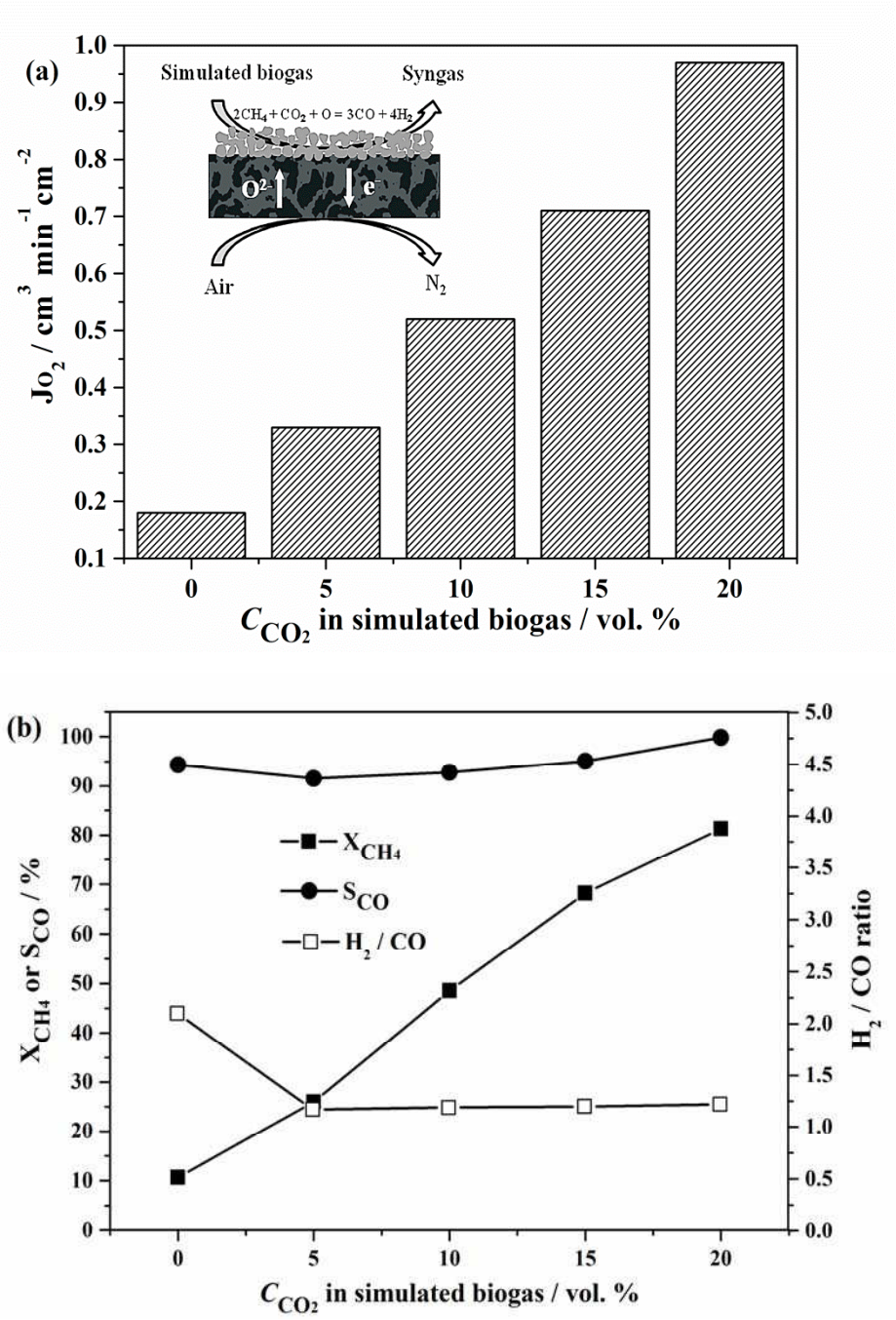

Figure 5. Oxygen permeation fluxes (a), CH_4 conversion (X_{CH4}), CO selectivity (S_{CO}) and H_2/CO ratio (b) through 0.7 mm thick membrane by exposing one side to air (100 cm^3 min^{-1}) and the other side to He-CH_4-CO_2 (total 20 cm^3 min^{-1}) with a CH_4 concentration of 30% and a CO_2 concentration of 0%, 5%, 10%, 15% and 20%. Temperature: 850 ˚C.

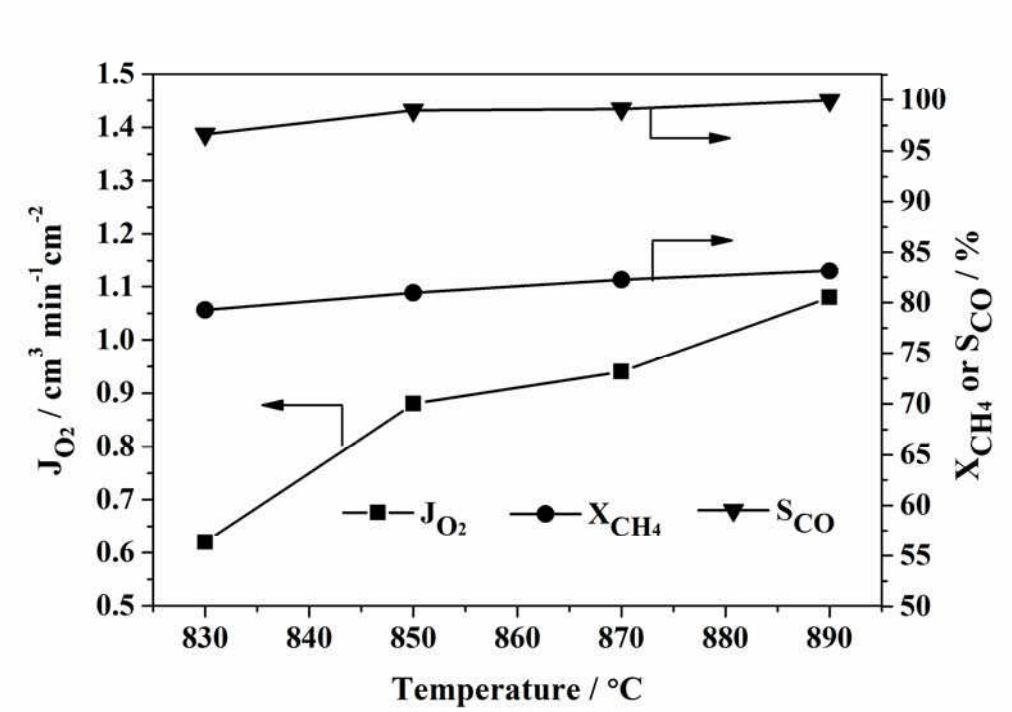

Figure 6. Influence of temperature on the CH_4 conversion (X_{CH4}), CO selectivity (S_{CO}), and oxygen permeation flux (J_{O2}) through the 60CGO−40GSFT dual phase membrane in the coupling of biogas reforming and air separation. Conditions: 100 cm^3 min^{-1} air as feed gas, 20 cm^3 min^{-1} simulated biogas (He-CH_4-CO_2) as sweep gas with CH_4 concentration of 30% and CO_2 concentration of 20%. Membrane thickness: 0.7 mm.

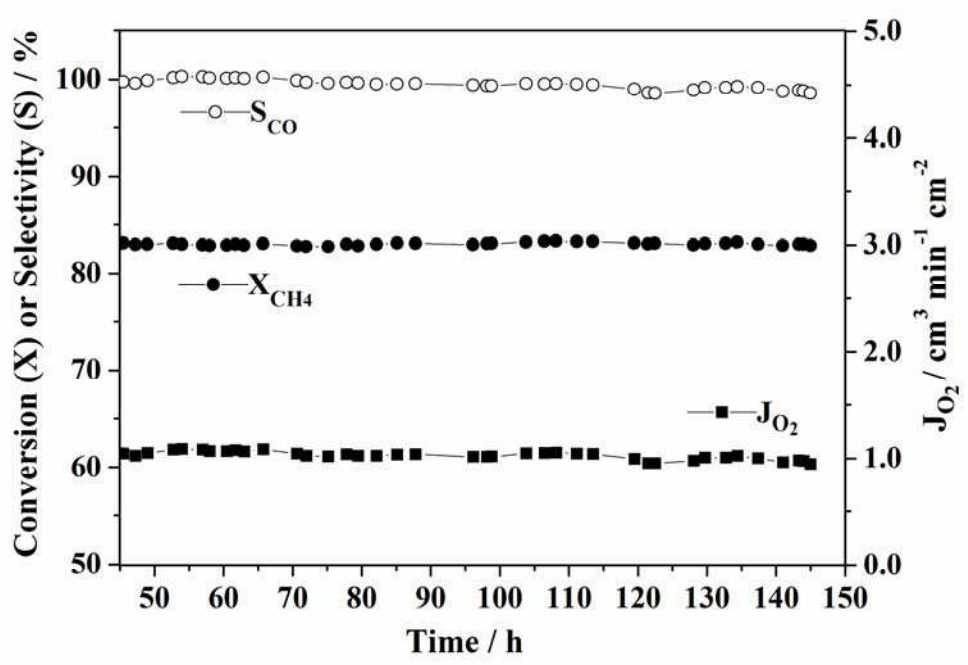

Figure 7. Time-dependence of CH_4 conversion (X_{CH4}), CO selectivity (S_{CO}) and oxygen permeation flux (J_{O2}) in the CGO−GSFT dual phase membrane reactor, Conditions: 100 cm^3 min^{-1} air as feed gas, 20 cm^3 min^{-1} simulated biogas (He-CH_4-CO_2) as sweep gas with CH_4 concentration of 30% and CO_2 concentration of 20%. Membrane thickness: 0.7 mm, Temperature: 890 ˚C.

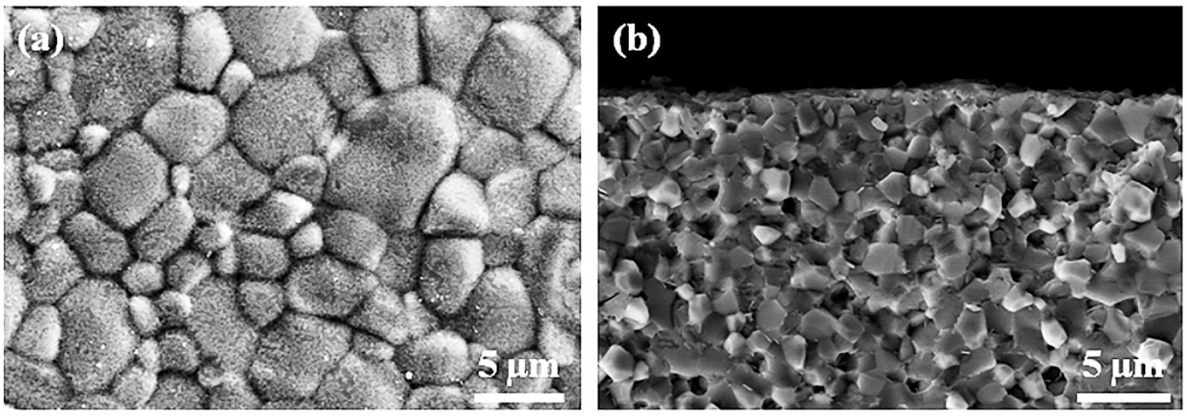

Figure 8. The SEM micrographs of the membrane surface on the biogas side (a) and cross-section (b) of the spent membrane exposed to air after biogas reforming for nearly 150 h.

For Table of Contents Only